Supporting Information for:

Specific Anion Effects for Aggregation of Colloidal Minerals: A Joint Experimental and Theoretical Study

Rui Tian, [†,‡] Gang Yang, [*,†] Chang Zhu, [†] Xinmin Liu, [†,‡] Hang Li[*,†]

[†]*College of Resources and Environment & Chongqing Key Laboratory of Soil Multi-scale Interfacial Process* and [‡]*College of Chemistry and Chemical Engineering, Southwest University, Chongqing 400715, China*

* To whom correspondence should be addressed:

E-mails: theobiochem@gmail.com; lihangswu@163.com;

Phone: 086-023-68251504; Fax: 086-023-68250444.

Contents:

S1. Choice of pH values for colloidal minerals

In addition to pH = 8.5 reported in the text, the aggregation kinetics of colloidal minerals are also investigated at pH = 7.0, 8.0, 9.0, and 10.0. Figures S1 ~ S4 show the time-evolution hydrodynamic diameters in $NaNO_3$ and KNO_3 solutions as well as the TAA rates $\tilde{\nu}_T(c_0)$ against electrolyte concentration c_0. The *CCC* values of pH = 7.0, 8.0, 8.5, 9.0, and 10.0 are equal to 71.7, 70.2, 71.1, 70.2 and 71.1 mmol/L in $NaNO_3$ solutions and 33.9, 35.3, 34.4, 34.3 and 32.4 mmol/L in KNO_3 solutions, respectively. For such a wide range of pH variations, the *CCC* values are very close to each other; moreover, in either solution, no consistent change trends vs. the increase or decrease of pH values can be detected. These explicitly validate the choice of pH = 8.5 for the aggregation studies.

Then the activation energies $\Delta E(c_0)$ for the aggregation of colloidal minerals in $NaNO_3$ and KNO_3 solutions with pH = 7.0, 8.0, 8.5, 9.0 and 10.0 are then calculated. Figures S5 and S6 indicate that for either $NaNO_3$ or KNO_3 solution, the $\Delta E(c_0)$ plots at these different pH values can be almost duplicate. For example, at 15.0 mmol/L, the $\Delta E(c_0)$ values at pH = 7.0, 8.0, 8.5, 9.0 and 10.0 are 1.59*RT*, 1.61*RT*, 1.66*RT*, 1.56*RT* and 1.58*RT* for $NaNO_3$ solutions and 0.30*RT*, 0.30*RT*, 0.30*RT*, 0.28*RT* and 0.27*RT* for KNO_3 solutions, respectively. This further substantializes the rationality of choosing pH = 8.5 for experiments as described in the text.

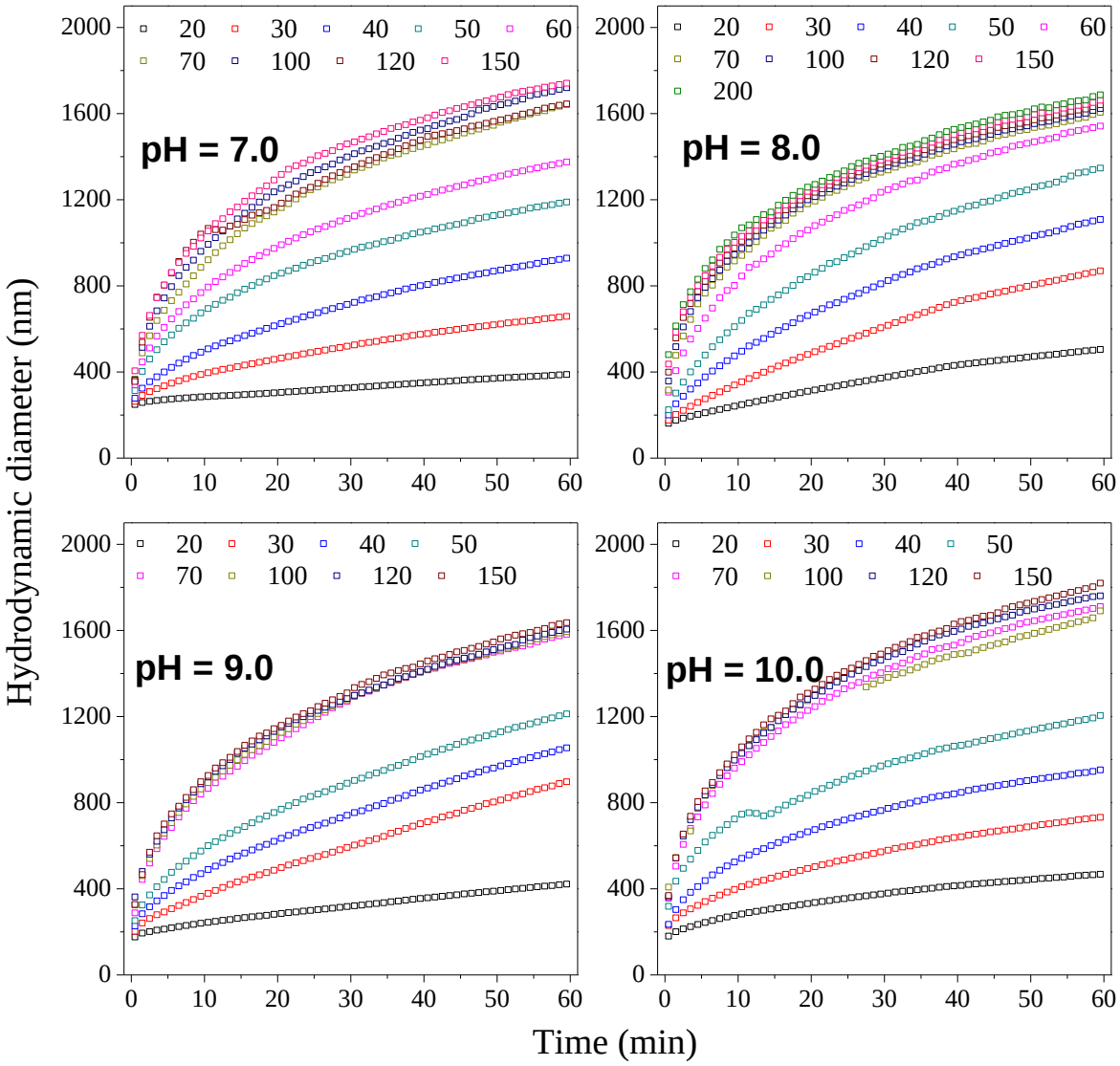

Figure S1. Time-evolution hydrodynamic diameters of colloidal minerals in $NaNO_3$ solutions at pH = 7.0, 8.0, 9.0 and 10.0. The electrolyte concentrations (mmol/L) are indicated in the legend.

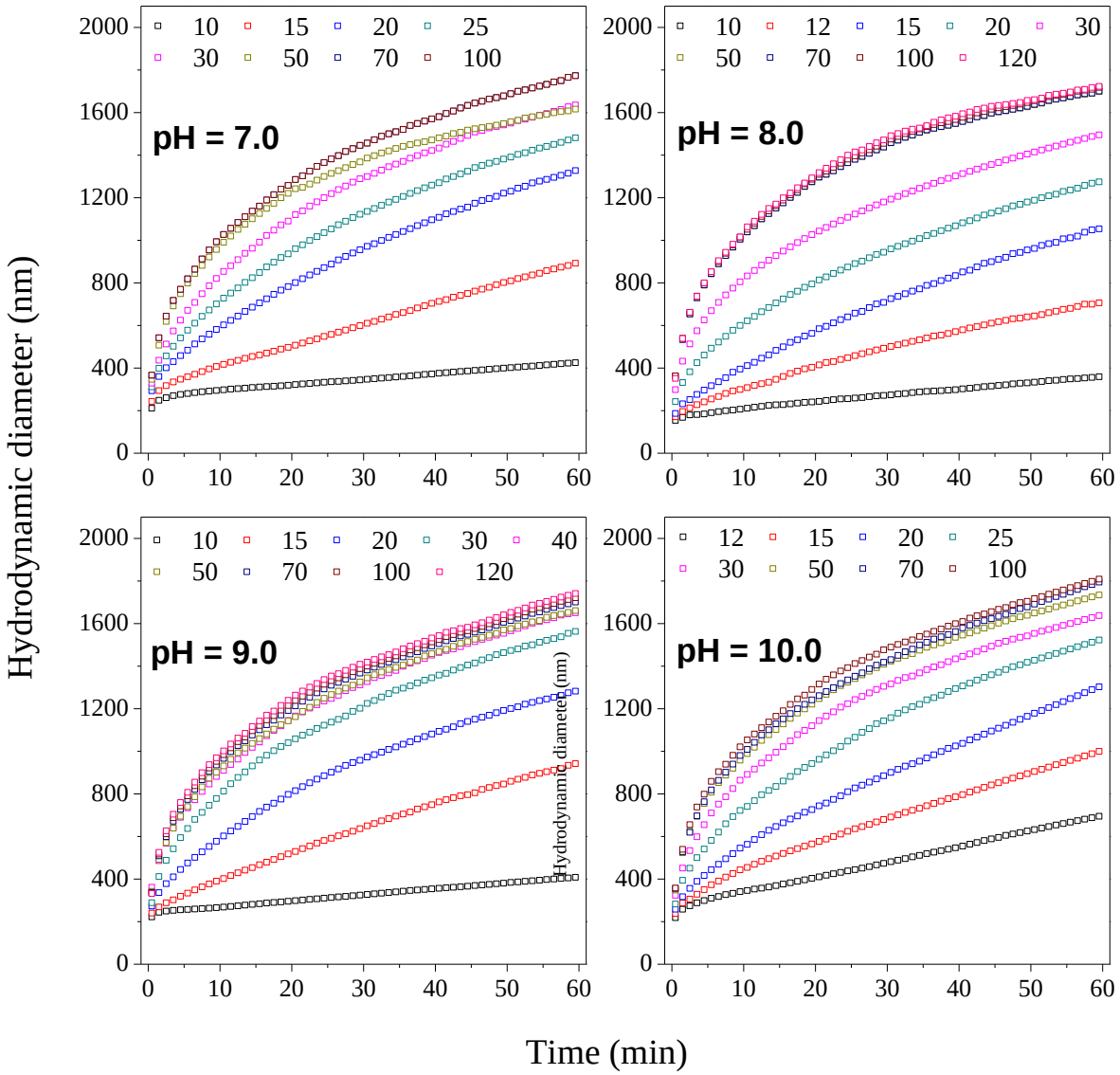

Figure S2. Time-evolution hydrodynamic diameters of colloidal minerals in KNO_3 solutions at pH = 7.0, 8.0, 9.0 and 10.0. The electrolyte concentrations (mmol/L) are indicated in the legend.

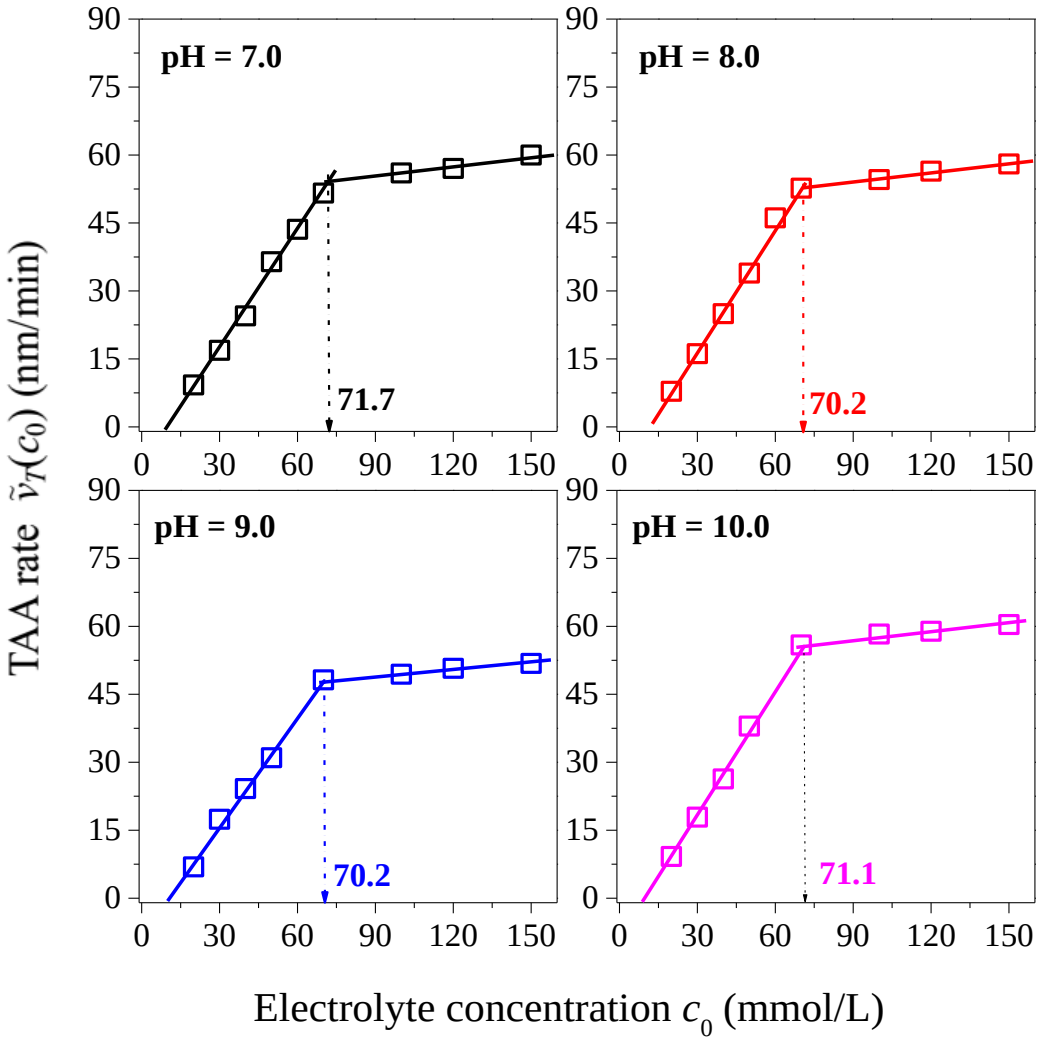

Figure S3. Changes of TAA rate $\tilde{v}_T(c_0)$ vs. electrolyte concentration c_0 for the aggregation of colloidal minerals in $NaNO_3$ solutions at pH = 7.0, 8.0, 9.0, and 10.0.

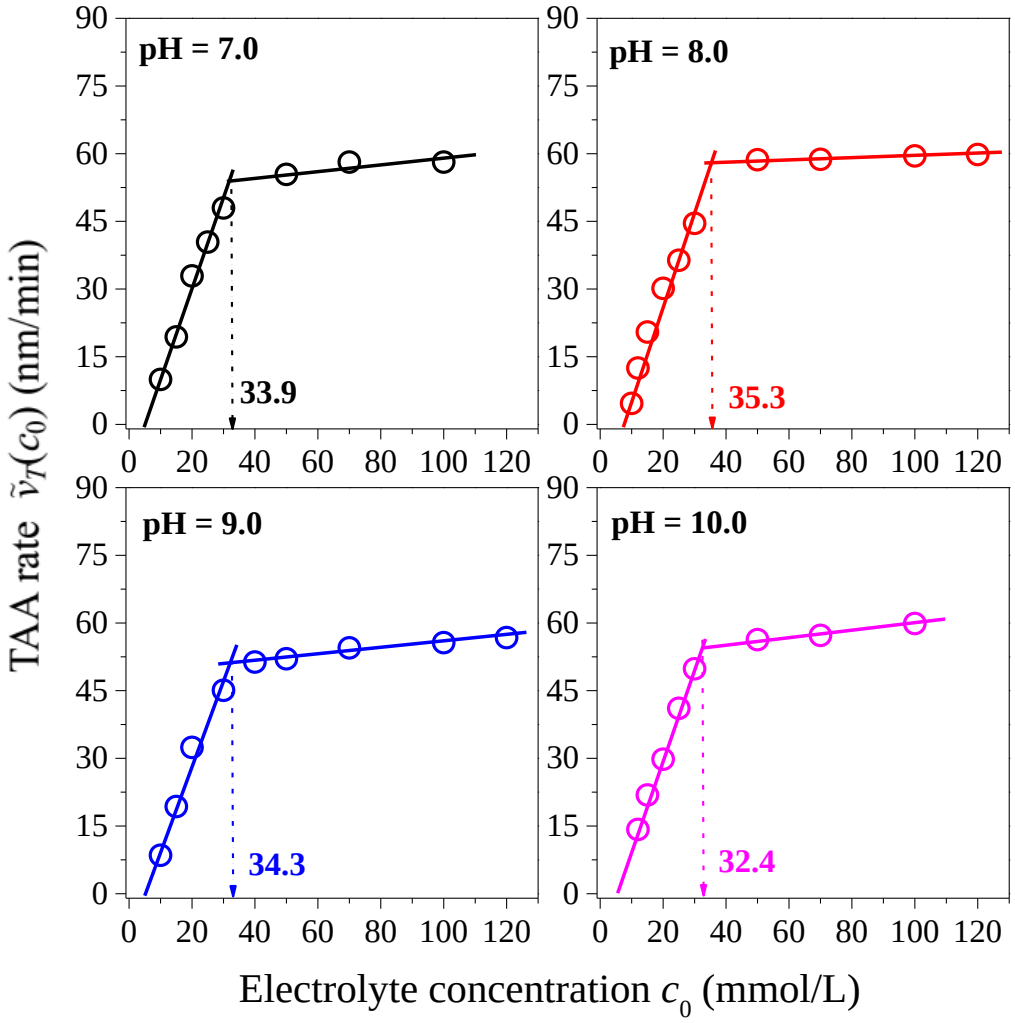

Figure S4. Changes of TAA rate $\tilde{v}_T(c_0)$ vs. electrolyte concentration c_0 for the aggregation of colloidal minerals in KNO_3 solutions at pH = 7.0, 8.0, 9.0, and 10.0.

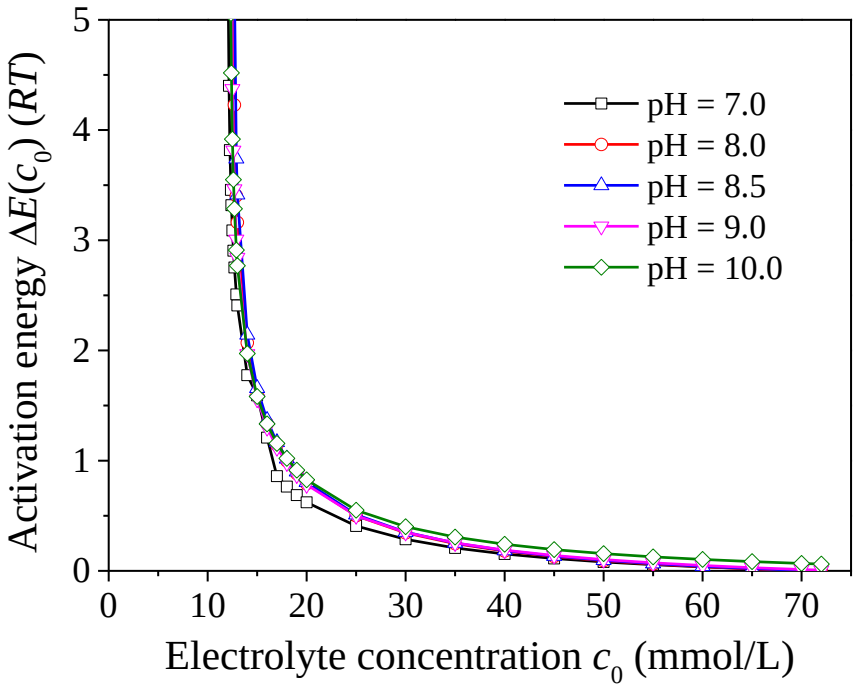

Figure S5. Activation energies $\Delta E(c_0)$ for the aggregation of colloidal minerals in $NaNO_3$ solutions at pH = 7.0, 8.0, 9.0, and 10.0.

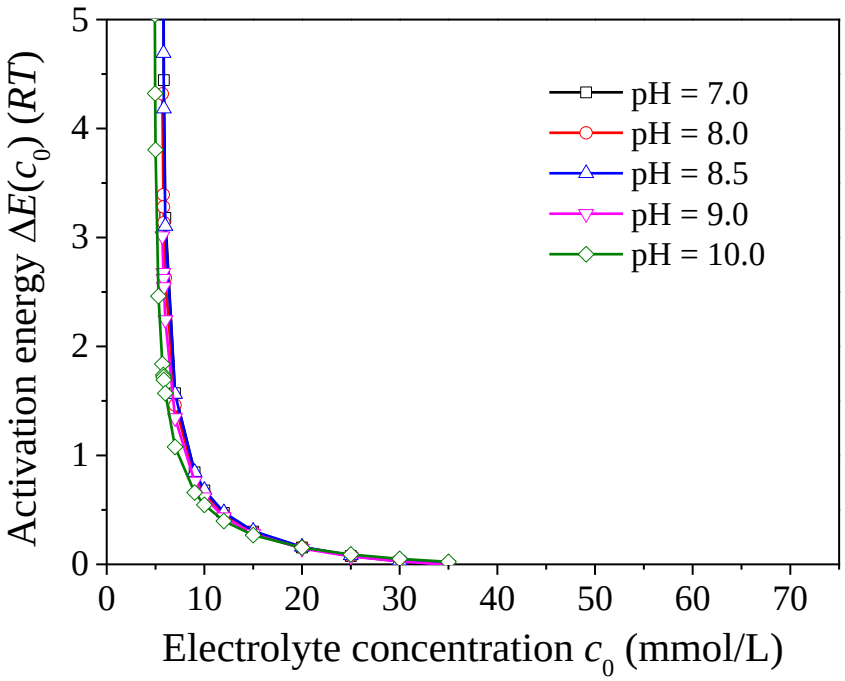

Figure S6. Activation energies $\Delta E(c_0)$ for the aggregation of colloidal minerals in KNO_3 solutions at pH = 7.0, 8.0, 9.0, and 10.0.

S2. Reproducibility of experimental results

For each sample, the DLS experiments reported in the text have been repeated two times, and here KNO_3 solutions were illustrated to demonstrate the reproducibility of experimental data. Based on the results of hydrodynamic diameter growths (Figure S7), the TAA rates $\tilde{\nu}_T(c_0)$ are calculated against the electrolyte concentrations (c_0) and shown in Figure S8. The *CCC* values of these three parallel experiments are rather close to each other, equaling 34.9, 34.6, and 34.7 mmol/L for KNO_3, respectively. The corresponding TAA rates below *CCC* are expressed as,

$$\tilde{\nu}_T(c_0) = 1.898c_0 - 10.96 \qquad (R^2 = 0.98) \qquad \text{(S1)}$$

$$\tilde{\nu}_T(c_0) = 1.849c_0 - 11.42 \qquad (R^2 = 0.99) \qquad \text{(S2)}$$

$$\tilde{\nu}_T(c_0) = 1.909c_0 - 11.30 \qquad (R^2 = 0.99) \qquad \text{(S3)}$$

The coefficients of determination (R^2) of the above equations show that in each DLS experiment, the linear relationship of TAA rates (below *CCC*) are quite satisfactory. The error bars (i.e., standard deviations) of TAA rates obtained from three parallel DLS experiments are shown in Figure S9, where the error bars are very small and even difficult to discern. That is, the data of different DLS experiments have a good reproducibility and those reported in the text are accurate.

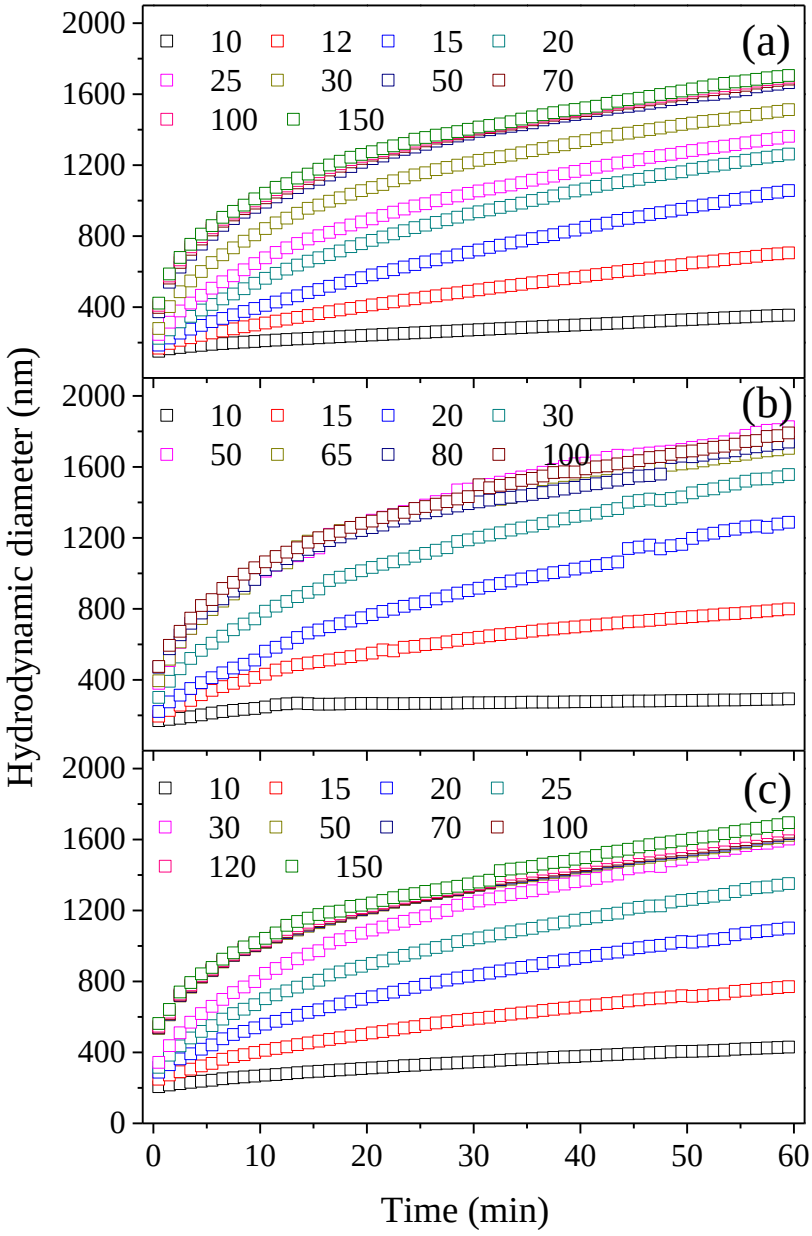

Figure S7. Time-evolution hydrodynamic diameters of colloidal minerals in KNO_3 solutions corresponding to three parallel DLS measurements. The electrolyte concentrations (mmol/L) are indicated in the legend.

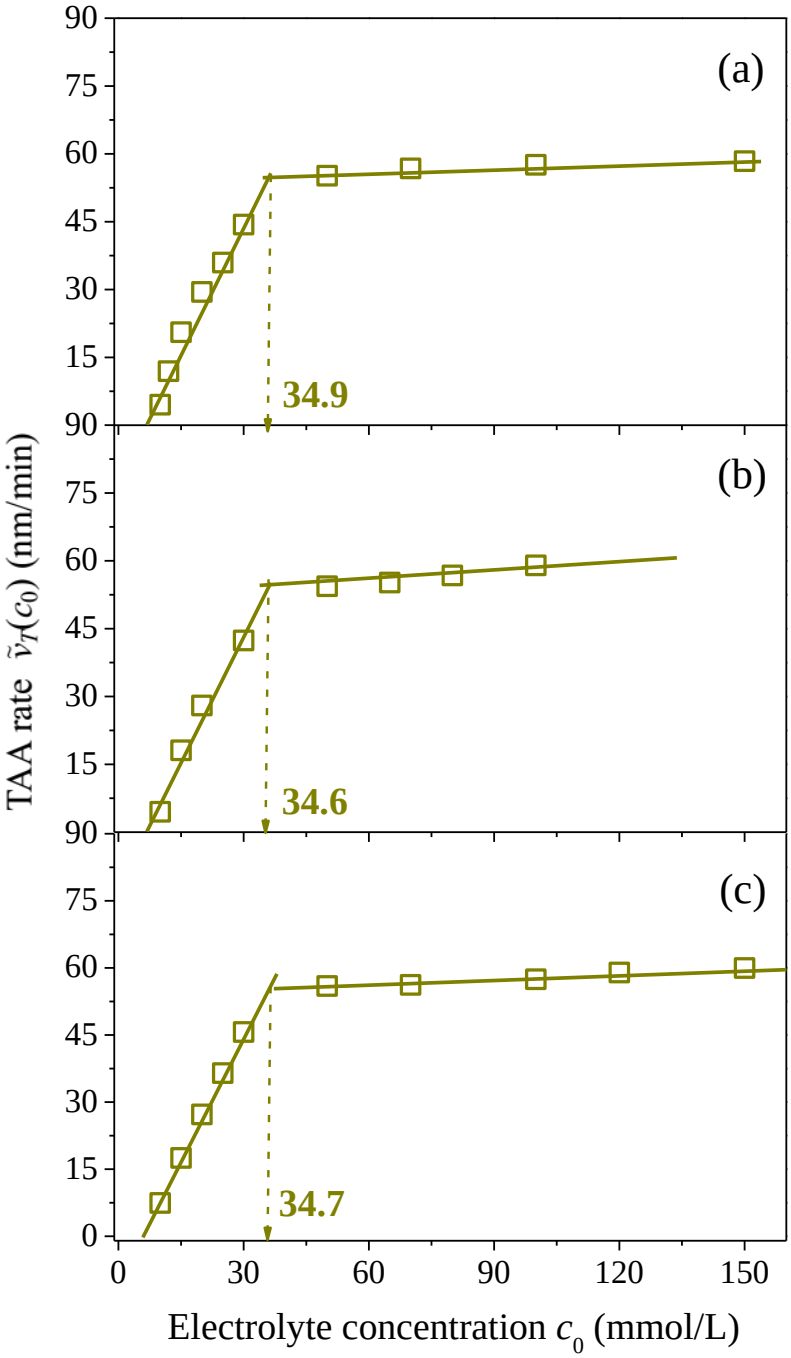

Figure S8. Changes of the TAA rate $\tilde{\nu}_T(c_0)$ vs. electrolyte concentration c_0 for the aggregation of colloidal minerals in KNO_3 solutions corresponding to three parallel DLS measurements.

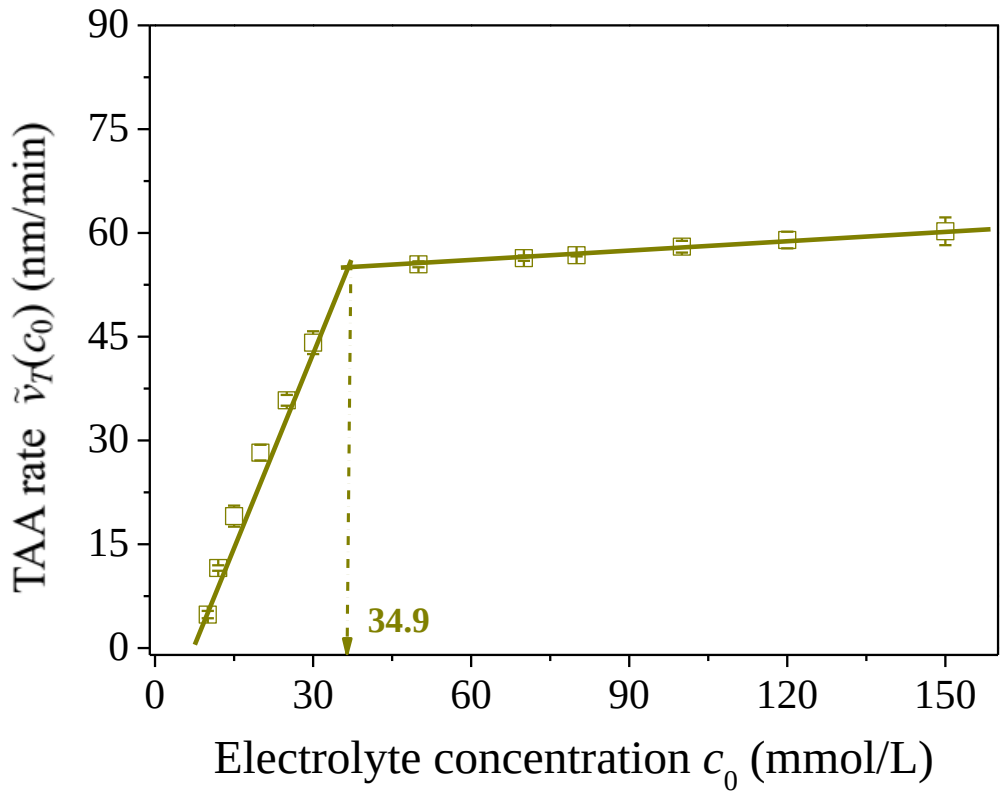

Figure S9. Changes of TAA rates $\tilde{v}_T(c_0)$ vs. electrolyte concentration c_0 for the aggregation of colloidal minerals in KNO_3 solutions, where the error bars (i.e., standard deviations) are derived from three parallel DLS measurements.

S3. Size distribution characteristics of colloidal aggregates

In the text, we report the average particle sizes (i.e., hydrodynamic diameters) of colloidal minerals in electrolyte solutions. At any specified time (t), the particles of colloidal minerals have a size distribution, and such information can be provided by use of the CONTIN algorithm.[1] The inset plots in Figure S10 indicate the size distributions in 100 mmol/L NaCl solutions at t = 0.5, 30, and 60 min. It can be seen that the colloidal aggregates have a rather narrow size distribution at the initial stage, and the polydispersive characteristics becomes more conspicuous with the increase of aggregation time (t), which are consistent with the aggregation results of fullerene nanoparticles.[1] In addition, at any specified time (t), the particle size of colloidal minerals has a Gaussian distribution and this suggests that all particles should be involved in the aggregation process. The size distributions in other electrolyte solutions as shown in Figures S11 ~ S15 can be analyzed in a similar way. Although the colloidal particles at any specified time (t) have a size distribution, the hydrodynamic diameters that respond promptly as the aggregation proceeds are sufficient to describe the aggregation kinetics, as reported else.[1-11]

References:

1. Meng, Z.; Hashmi, S. M.; Elimelech, M. Aggregation Rate and Fractal Dimension of Fullerene Nanoparticles via Simultaneous Multiangle Static and Dynamic Light Scattering Measurement. *J. Colloid Interface Sci.* **2013,** *392*, 27-33.

2. Sandkuhler, P.; Sefcik, J.; Morbidelli, M., Kinetics of Aggregation and Gel Formation in Concentrated Polystyrene Colloids. *J. Phys. Chem. B* **2004,** *108*, 20105-20121.

3. Korala, L.; Brock, S. L. Aggregation Kinetics of Metal Chalcogenide Nanocrystals: Generation of Transparent CdSe (ZnS) Core (Shell) Gels. *J. Phys. Chem. C* **2012,** *116*, 17110-17117.

4. Tian, R.; Yang, G.; Li, H.; Gao, X. D.; Liu, X. M.; Zhu, H. L.; Tang, Y. Activation Energies of Colloidal Particle Aggregation: Towards a Quantitative Characterization of Specific Ion Effects. *Phys. Chem. Chem. Phys.* **2014,** *16*, 8828 - 8836.

5. Missel, P. J.; Mazer, N. A.; Carey, M. C.; Benedek, G. B., Influence of Alkali-Metal Counterion Identity on the Sphere-to-Rod Transition in Alkyl Sulfate Micelles. *J. Phys. Chem.* **1989,** *93*, 8354-8366.

6. Baldyga, J.; Jasinska, M.; Jodko, K.; Petelski, P. Precipitation of Amorphous Colloidal Silica from Aqueous Solutions-Aggregation Problem. *Chem. Eng. Sci.* **2012,** *77*, 207-216.

7. Porte, G.; Appell, J. Growth and Size Distributions of Cetylpridlnium Bromide Micelles in High Ionic Strength Aqueous Solutions. *J. Phys. Chem.* **1981,** *85*, 2511-2519.8. Bouchard, D.; Ma, X.; Issacson, C. Colloidal Properties of Aqueous Fullerenes: Isoelectric Points and Aggregation Kinetics of C_{60} and C_{60} Derivatives. *Environ. Sci. Technol.* **2009,** *43*, 6597-6603.

9. Jin, Z. L.; Hou, W. G.; Sun, D. J.; Zhang, C. G. Studies on Kinetic Behaviour of Colloidal Dispersion of Mg-Al Hydrotalcite-like Compounds. *Indian J. Chem. A* **2006,** *45*, 609-613.

10. Sousa, V. S.; Teixeira, M. R. Aggregation Kinetics and Surface Charge of CuO Nanoparticles: the Influence of pH, Ionic Strength and Humic Acids. *Environ. Chem.* **2013,** *10*, 313-322.

11. Cini, N.; Tulun, T.; Blanck, C.; Toniazzo, V.; Ruch, D.; Decher, G.; Ball, V. Slow Complexation Dynamics between Linear Short Polyphosphates and Polyallylamines: Analogies with "layer-by-layer" Deposits. *Phys. Chem. Chem. Phys.* **2012,** *14*, 3048-3056.

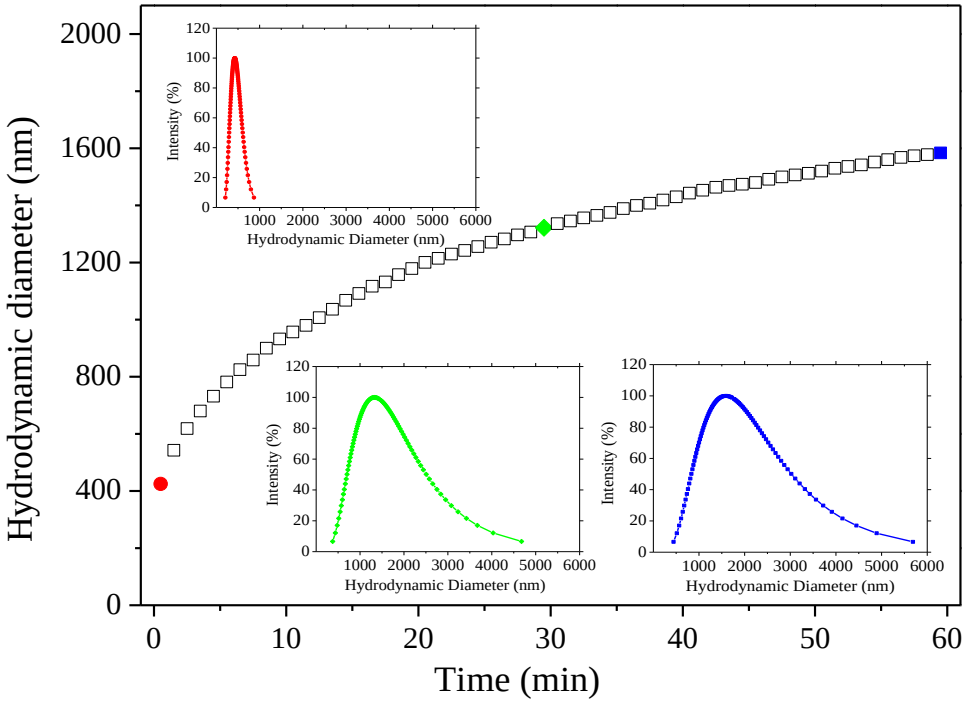

Figure S10. The average particle sizes of colloidal minerals vs. experimental time (*t*) in 100 mmol/L NaCl solutions. Inset plots represent the size distributions at *t* = 0.5 min (in red), *t* = 30 min (in green) and *t* = 60 min (in blue), respectively. The red, green, and blue data points in the main curve indicate the average particle sizes corresponding to each inset plot.

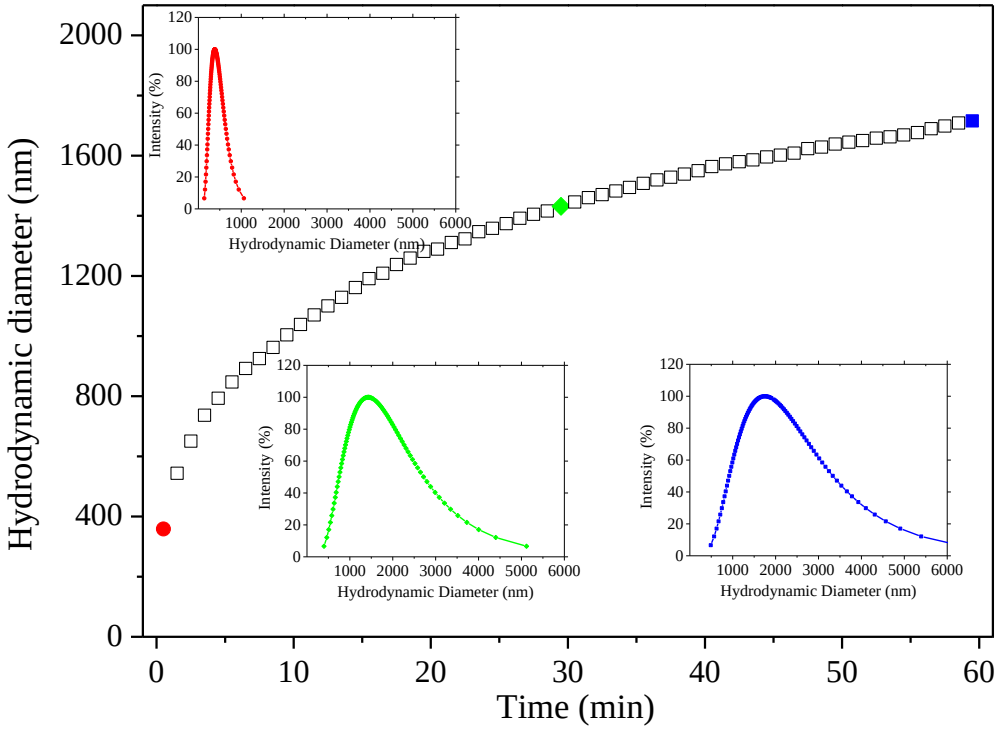

Figure S11. The average particle sizes of colloidal minerals vs. experimental time (*t*) in 100 mmol/L KCl solutions. Inset plots represent the size distributions at *t* = 0.5 min (in red), *t* = 30 min (in green) and *t* = 60 min (in blue), respectively. The red, green, and blue data points in the main curve indicate the average particle sizes corresponding to each inset plot.

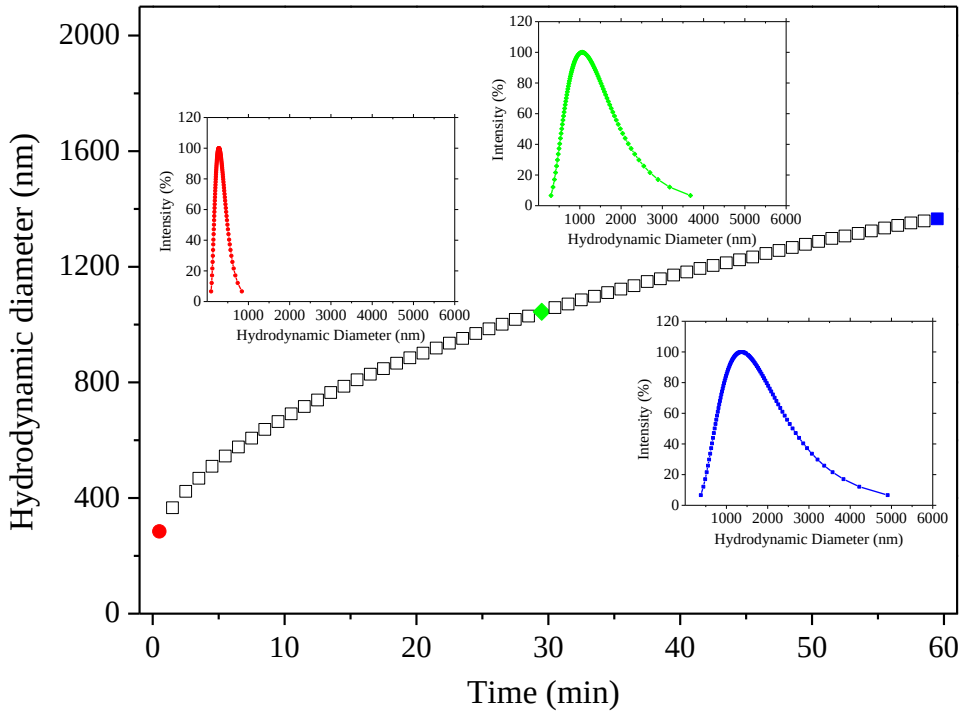

Figure S12. The average particle sizes of colloidal minerals vs. experimental time (*t*) in 50 mmol/L Na_2SO_4 solutions. Inset plots represent the size distributions at *t* = 0.5 min (in red), *t* = 30 min (in green) and *t* = 60 min (in blue), respectively. The red, green, and blue data points in the main curve indicate the average particle sizes corresponding to each inset plot.

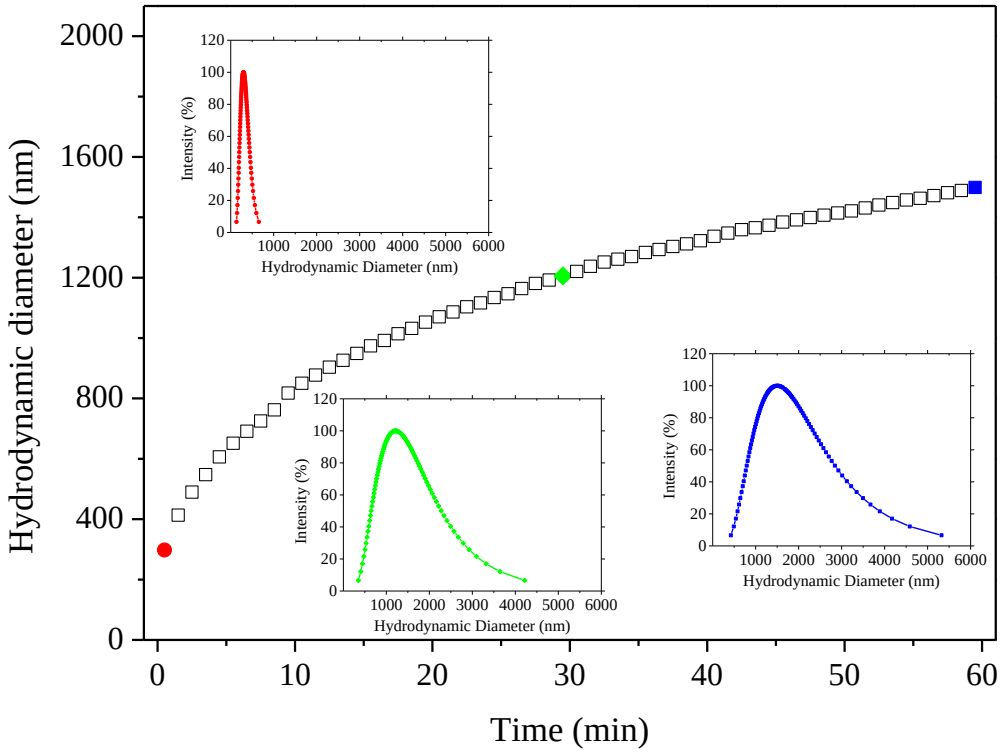

Figure S13. The average particle sizes of colloidal minerals vs. experimental time (*t*) in 50 mmol/L K_2SO_4 solutions. Inset plots represent the size distributions at *t* = 0.5 min (in red), *t* = 30 min (in green) and *t* = 60 min (in blue), respectively. The red, green, and blue data points in the main curve indicate the average particle sizes corresponding to each inset plot.

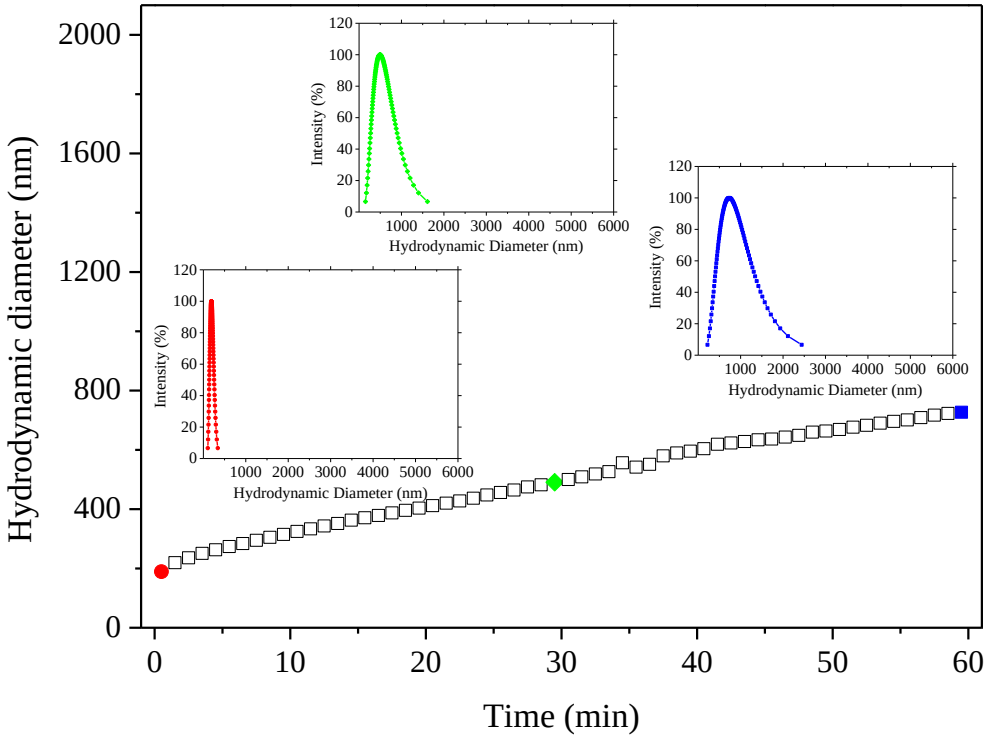

Figure S14. The average particle sizes of colloidal minerals vs. experimental time (*t*) in 100 mmol/L Na_3PO_4 solutions. Inset plots represent the size distributions at *t* = 0.5 min (in red), *t* = 30 min (in green) and *t* = 60 min (in blue), respectively. The red, green, and blue data points in the main curve indicate the average particle sizes corresponding to each inset plot.

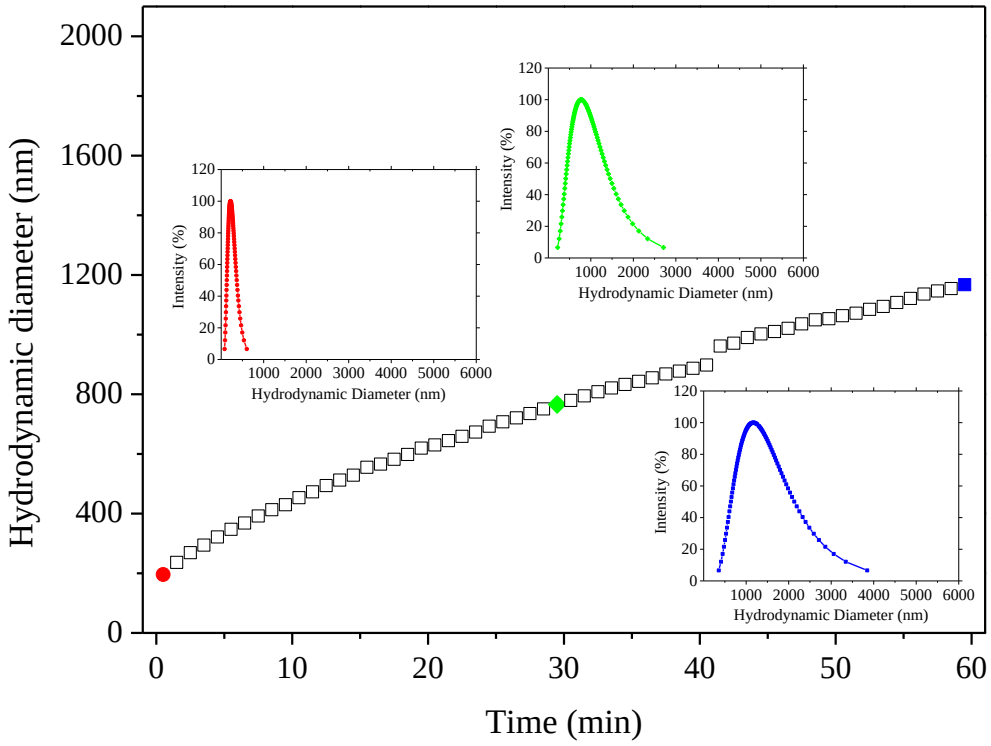

Figure S15. The average particle sizes of colloidal minerals vs. experimental time (*t*) in 100 mmol/L K_3PO_4 solutions. Inset plots represent the size distributions at *t* = 0.5 min (in red), *t* = 30 min (in green) and *t* = 60 min (in blue), respectively. The red, green, and blue data points in the main curve indicate the average particle sizes corresponding to each inset plot.

Table S1. Expressions of TAA rates $\tilde{\nu}_T(c_0)$ for the aggregation of colloidal minerals in $NaNO_3$, NaCl, KNO_3, KCl, Na_3PO_4, K_2HPO_4, K_3PO_4, KH_2PO_4, Na_2SO_4 and K_2SO_4 solutions [a,b]

Electrolyte solutions	$\tilde{\nu}_T(c_0) = (c_0 \leq CCC)$	R^2
$NaNO_3$	$0.917c_0-11.60$	0.99
NaCl	$0.919c_0-11.29$	0.99
KNO_3	$1.898c_0-10.96$	0.99
KCl	$1.892c_0-10.42$	0.98
Na_3PO_4	$0.376c_0-22.50$	0.99
K_2HPO_4	$0.474c_0-30.01$	0.99
K_3PO_4	$0.515c_0-29.37$	0.99
KH_2PO_4	$1.933c_0-5.42$	0.99
Na_2SO_4	$0.822c_0-6.03$	0.99
K_2SO_4	$1.391c_0-5.53$	0.98

[a] Units of $\tilde{\nu}_T(c_0)$ and *CCC* are nm/min and mmol/L, respectively;

[b] R^2 refers to the coefficient of determination.

Table S2. Expressions of activation energies $\Delta E(c_0)$ for the aggregation of colloidal minerals in Na_3PO_4, K_2HPO_4, K_3PO_4 and KH_2PO_4 solutions [a]

Electrolyte solutions (*CCC*)	$\Delta E(c_0) = (c_0 \leq CCC)$
Na_3PO_4 (203.1)	$-RT\ln(-84.73/c_0+1.417)$
K_2HPO_4 (173.6)	$-RT\ln(-99.58/c_0+1.573)$
K_3PO_4 (149.2)	$-RT\ln(-92.43/c_0+1.619)$
KH_2PO_4 (22.6)	$-RT\ln(-3.201/c_0+1.142)$

[a] Units of $\Delta E(c_0)$ and *CCC* are *RT* and mmol/L, respectively.

Table S3. pH change ranges (ΔpH) of electrolyte solutions during the aggregation processes of colloidal minerals[a]

KNO_3	c_0	10	12	15	20	25	30	50	70	100	150
	ΔpH	0.02	0.02	0.03	0.02	0.05	0.02	0.04	0.04	0.03	0.05
KCl	c_0	10	15	20	25	30	50	70	100	120	150
	ΔpH	0.01	0.02	0.03	0.05	0.02	0.02	0.04	0.07	0.03	0.05
K_2SO_4	c_0	5	10	15	20	30	50	70	100	150	200
	ΔpH	0.02	0.01	0.03	0.02	0.02	0.02	0.06	0.04	0.03	0.05
KH_2PO_4	c_0	5	7	10	15	20	40	50	100		
	ΔpH	0.02	0.04	0.01	0.03	0.04	0.05	0.08	0.02		
K_2HPO_4	c_0	80	100	120	150	200	250	300	500		
	ΔpH	0.03	0.02	0.05	0.02	0.07	0.04	0.03	0.06		
K_3PO_4	c_0	70	80	90	100	120	150	200	250		
	ΔpH	0.02	0.02	0.04	0.02	0.02	0.02	0.04	0.07		

[a] Unit of electrolyte concentrations (c_0) is mmol/L.

Table S4. Surface charge densities of colloidal aggregates in KH_2PO_4, KCl, KNO_3, K_2SO_4, K_2HPO_4, and K_3PO_4 solutions ($f_0(K^+)$ = 30 mmol/L)[a]

Electrolyte solutions	Surface charge densities
KH_2PO_4	0.138 ± 0.006
KCl	0.142 ± 0.002
KNO_3	0. 145 ± 0.003
K_2SO_4	0. 154 ± 0.004
K_2HPO_4	0.197 ± 0.003
K_3PO_4	0.255 ± 0.005

[a] Unit of surface charge densities is C/m^2.

Table S5. Surface charge densities of colloidal minerals in KOH solutions with different pH values[a]

pH	10.0	12.0	12.4
Surface charge densities	0.291 ± 0.002	0.304 ± 0.005	0.415 ± 0.007

[a] Unit of surface charge densities is C/m^2.

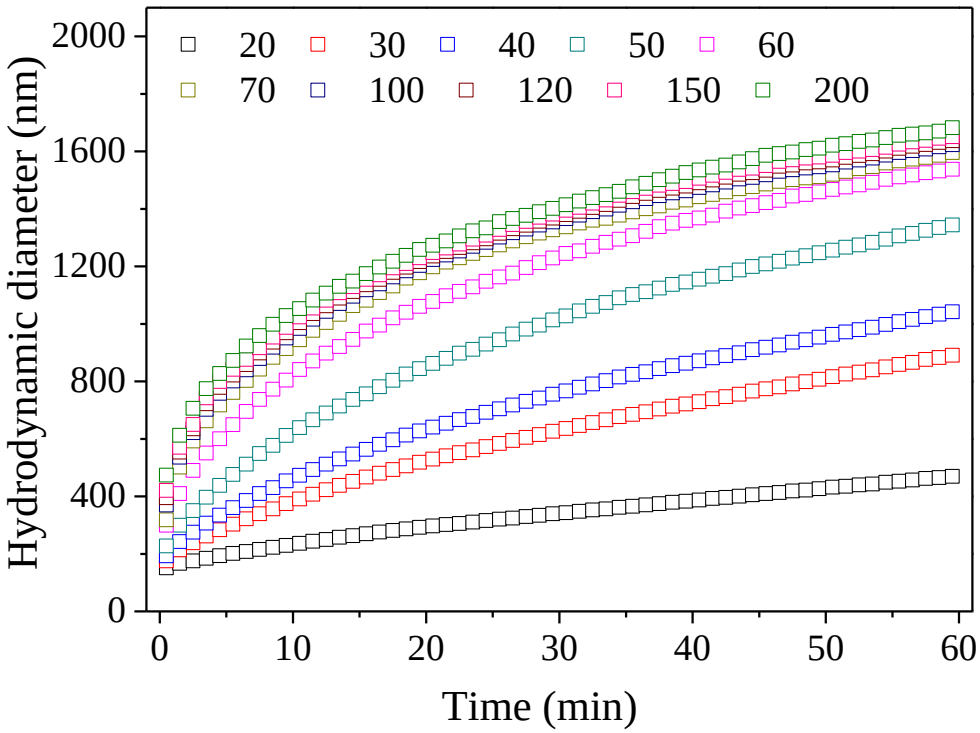

Figure S16. Time-evolution hydrodynamic diameters of colloidal minerals in $NaNO_3$ solutions. The electrolyte concentrations (mmol/L) are indicated in the legend.

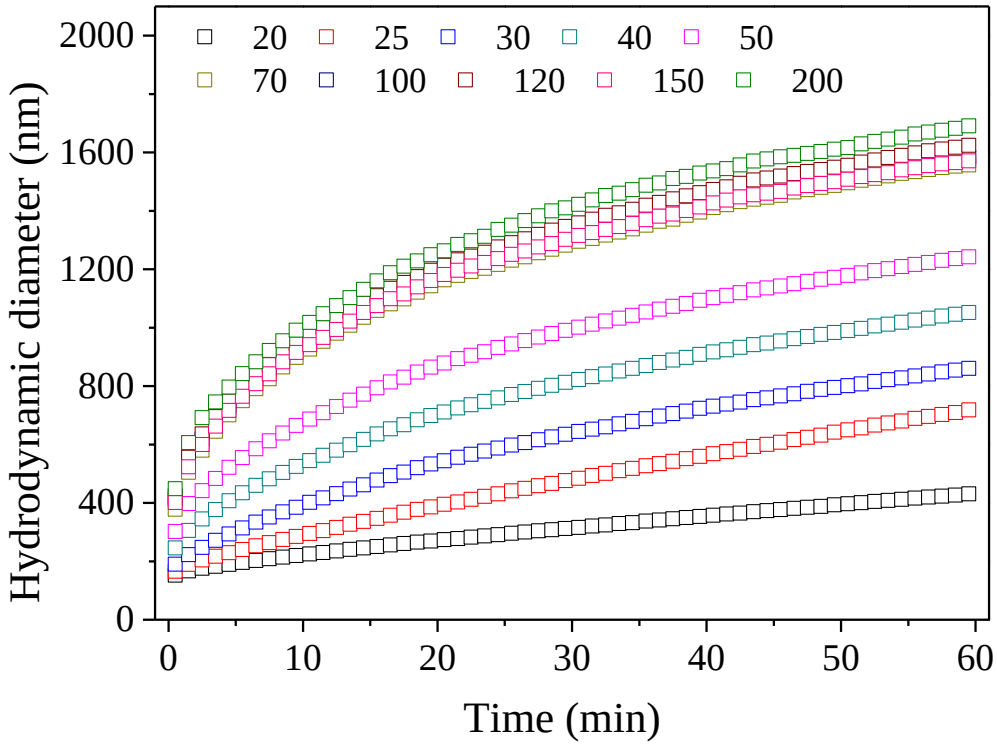

Figure S17. Time-evolution hydrodynamic diameters of colloidal minerals in NaCl solutions. The electrolyte concentrations (mmol/L) are indicated in the legend.

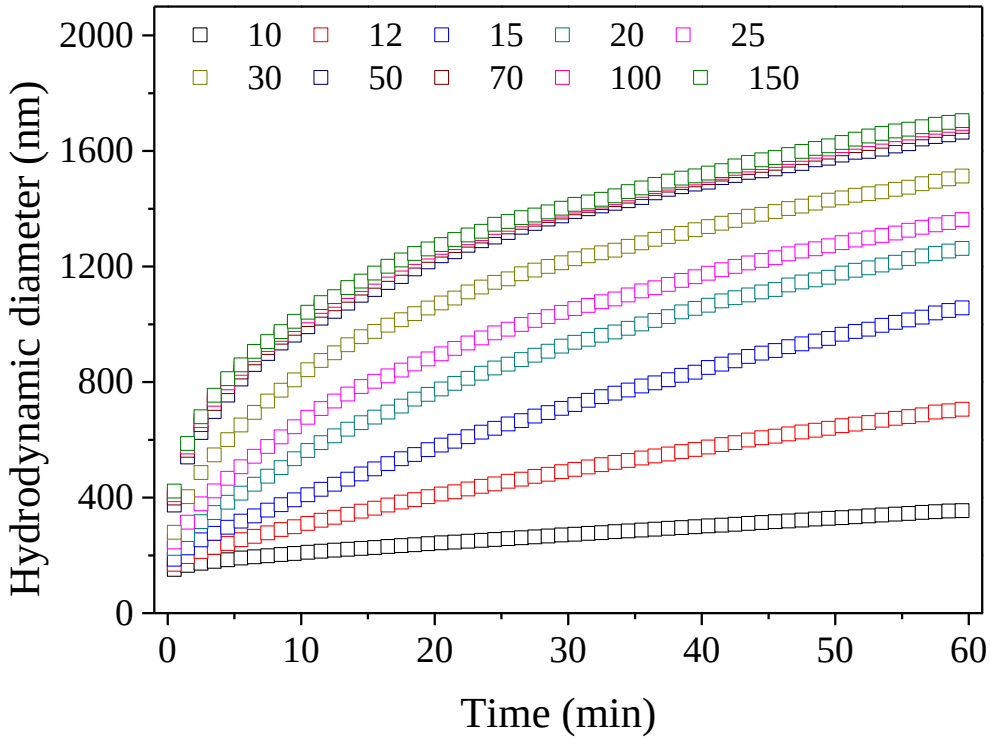

Figure S18. Time-evolution hydrodynamic diameters of colloidal minerals in KNO_3 solutions. The electrolyte concentrations (mmol/L) are indicated in the legend.

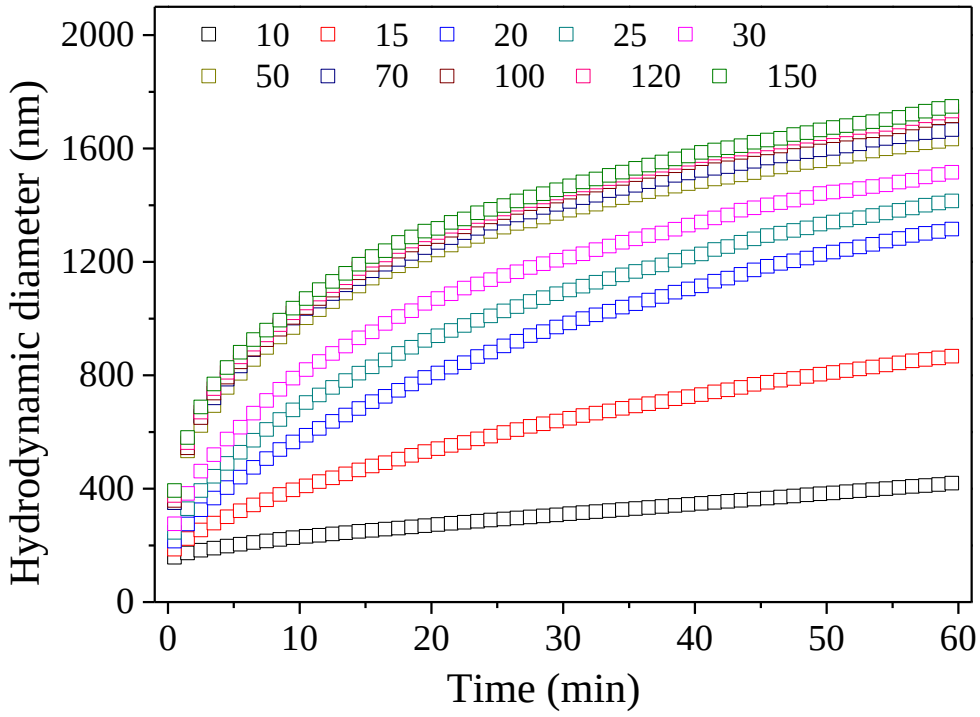

Figure S19. Time-evolution hydrodynamic diameters of colloidal minerals in KCl solutions. The electrolyte concentrations (mmol/L) are indicated in the legend.

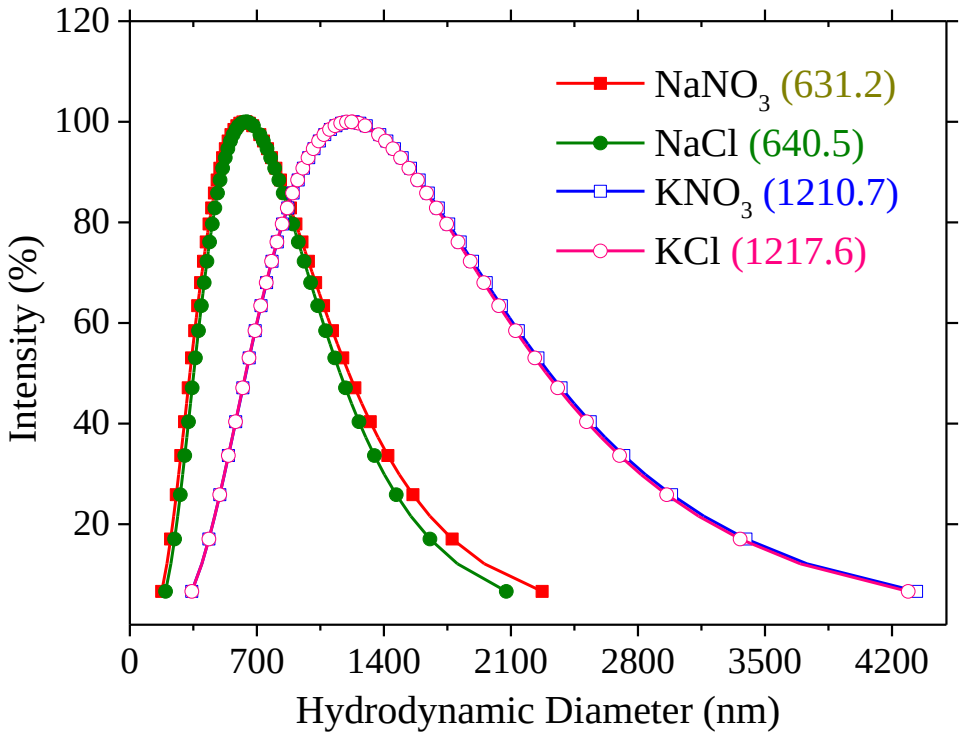

Figure S20. Size distributions of colloidal minerals at t = 30 min in 30 mmol/L $NaNO_3$, NaCl, KNO_3, and KCl solutions.

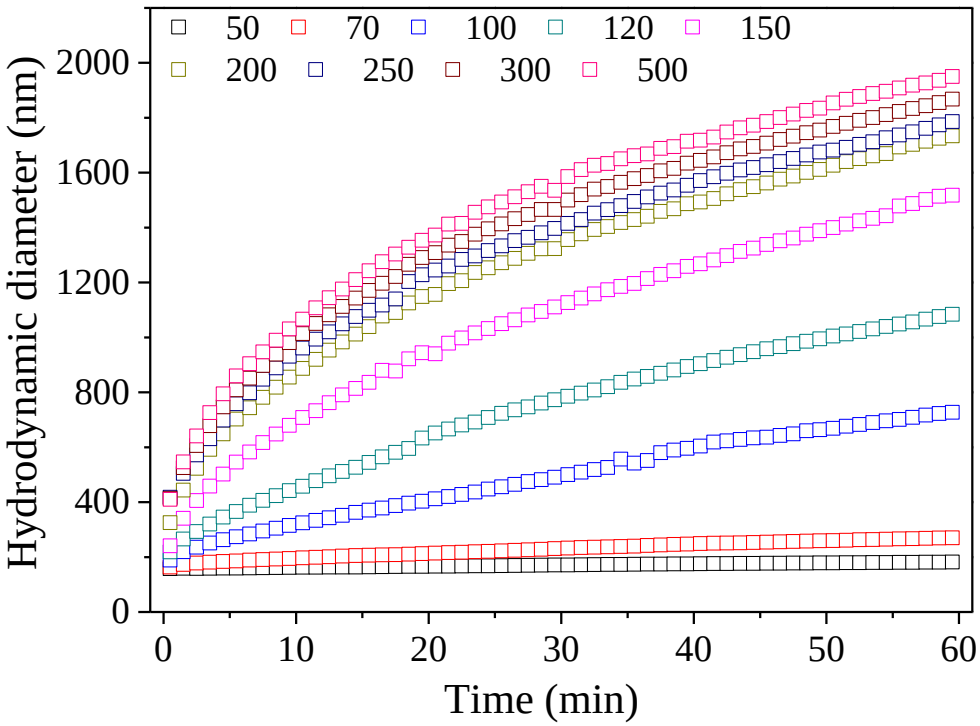

Figure S21. Time-evolution hydrodynamic diameters of colloidal minerals in Na_3PO_4 solutions. The electrolyte concentrations (mmol/L) are indicated in the legend.

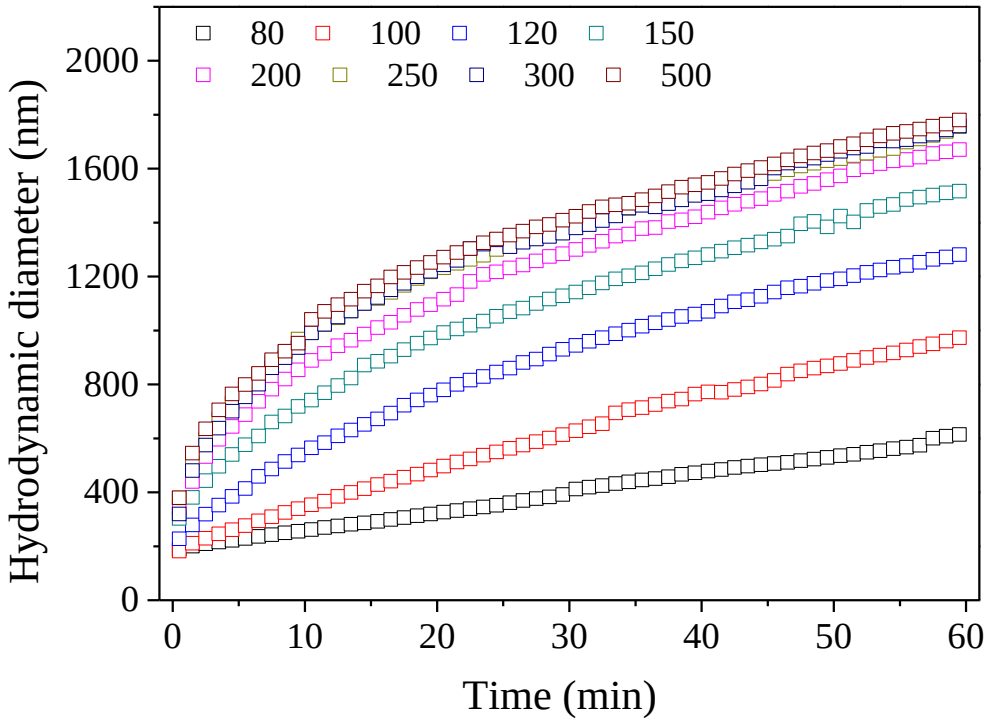

Figure S22. Time-evolution hydrodynamic diameters of colloidal minerals in K_2HPO_4 solutions. The electrolyte concentrations (mmol/L) are indicated in the legend.

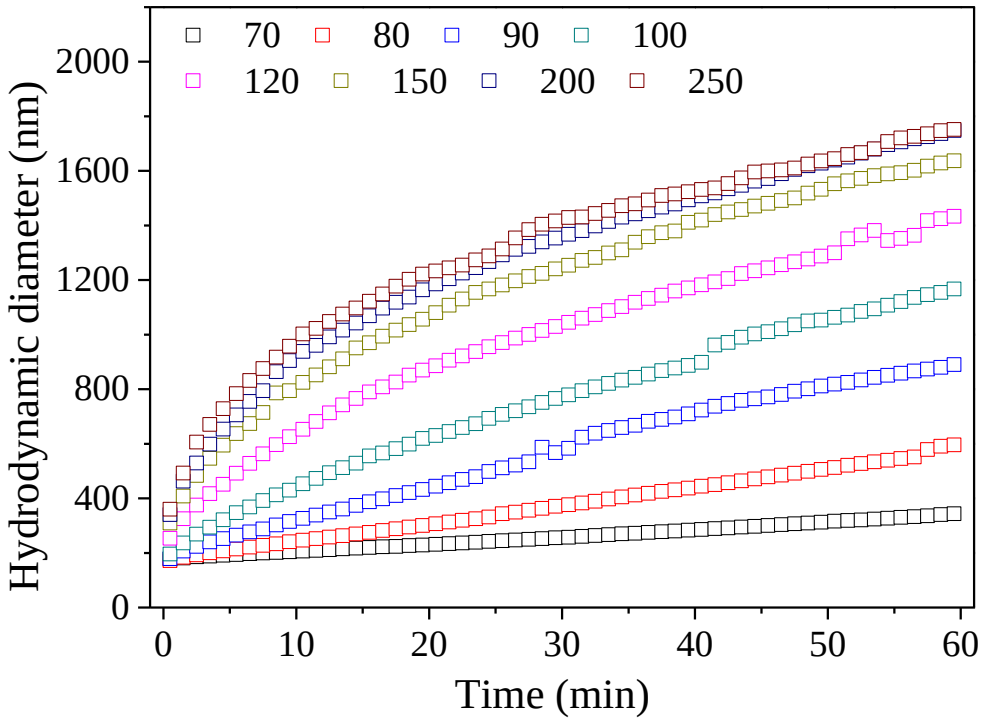

Figure S23. Time-evolution hydrodynamic diameters of colloidal minerals in K_3PO_4 solutions. The electrolyte concentrations (mmol/L) are indicated in the legend.

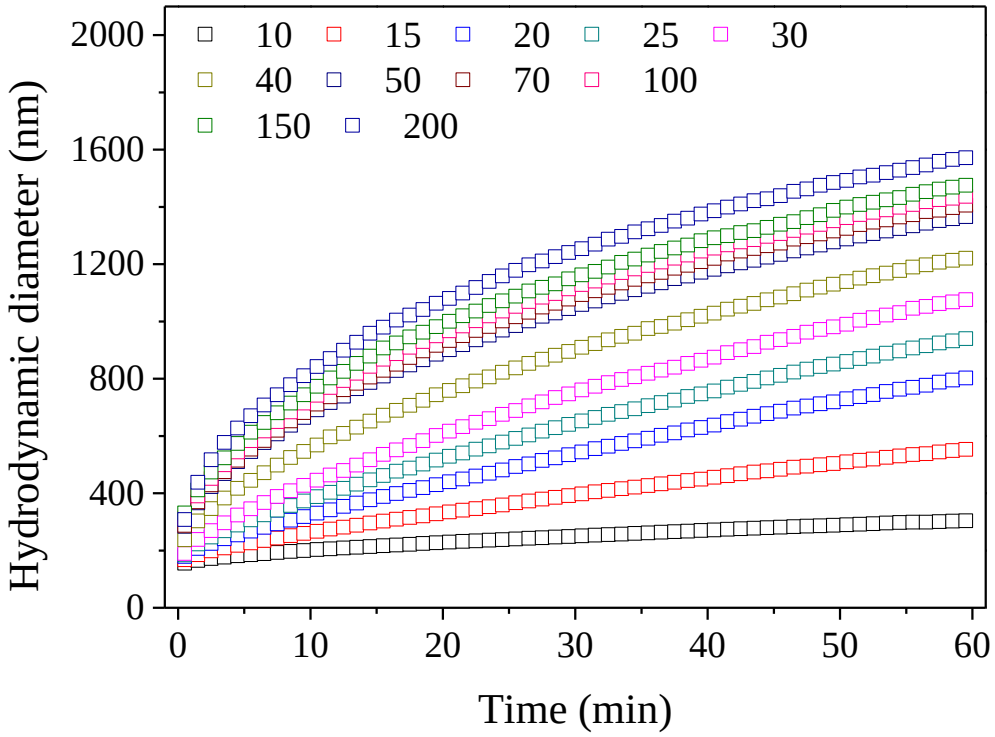

Figure S24. Time-evolution hydrodynamic diameters of colloidal minerals in Na_2SO_4 solutions. The electrolyte concentrations (mmol/L) are indicated in the legend.

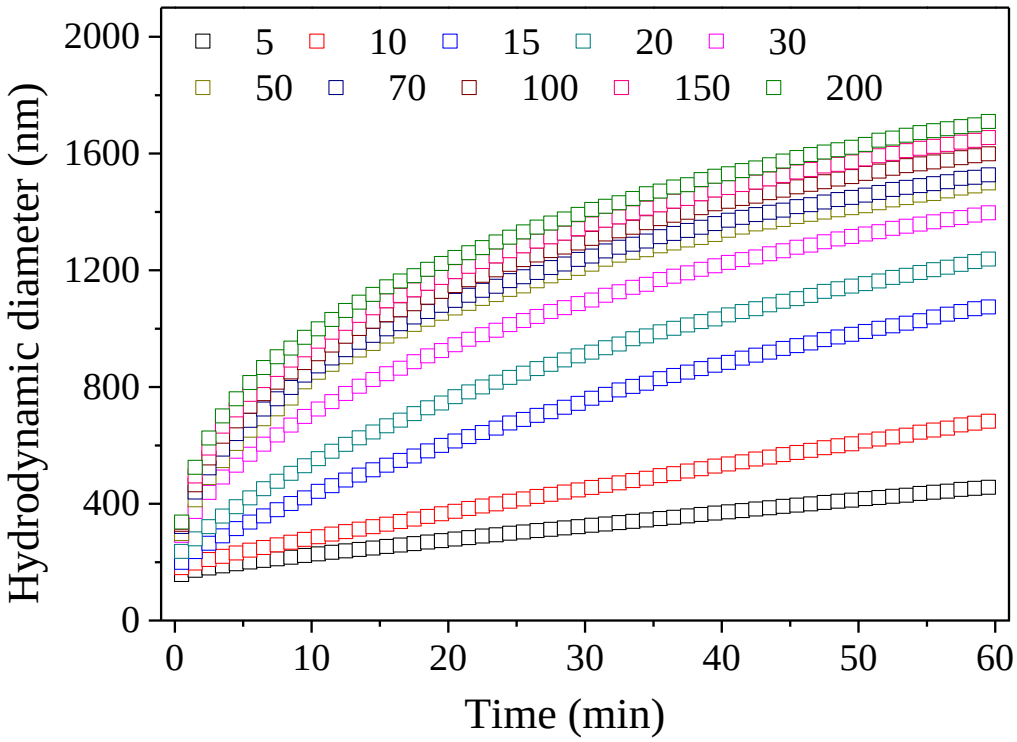

Figure S25. Time-evolution hydrodynamic diameters of colloidal minerals in K_2SO_4 solutions. The electrolyte concentrations (mmol/L) are indicated in the legend.

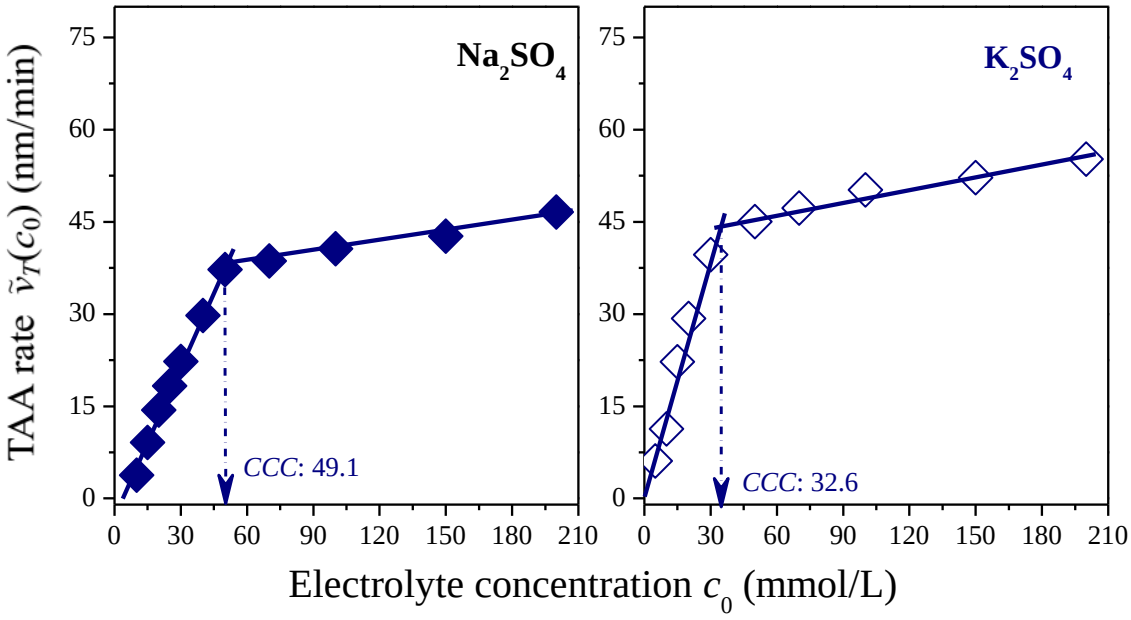

Figure S26. Changes of TAA rate $\tilde{v}_T(c_0)$ vs. electrolyte concentration c_0 for the aggregation of colloidal minerals in Na_2SO_4 and K_2SO_4 solutions.

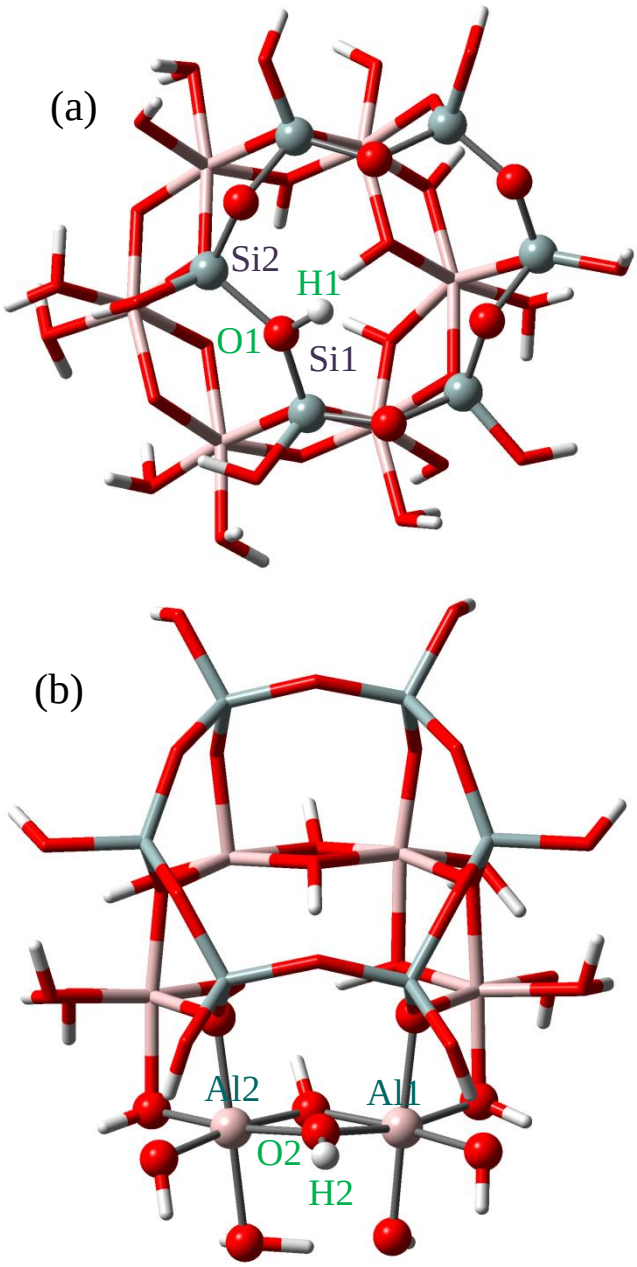

Figure S27. Protonated structures of (a) The hexagonal ring of silica surface and (b) O atoms of the $Al(O_2H)Al$ link in kaolinite mineral. The high-level regions are shown as ball and stick while the low-level regions as stick.

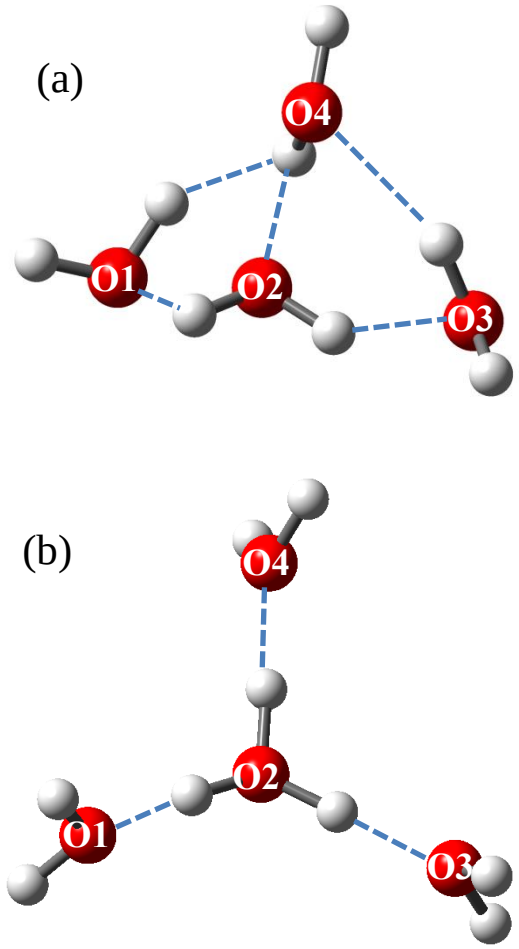

Figure S28. Structures of (a) water cluster $(H_2O)_4$ and (b) its protonated form $(H_9O_4)^+$ according to the work of Intharathep et al. (*J. Comput. Chem.* **2006**, *27*, 1723). The protonated form has been experimentally determined as the most prevalent species for a proton in solutions.

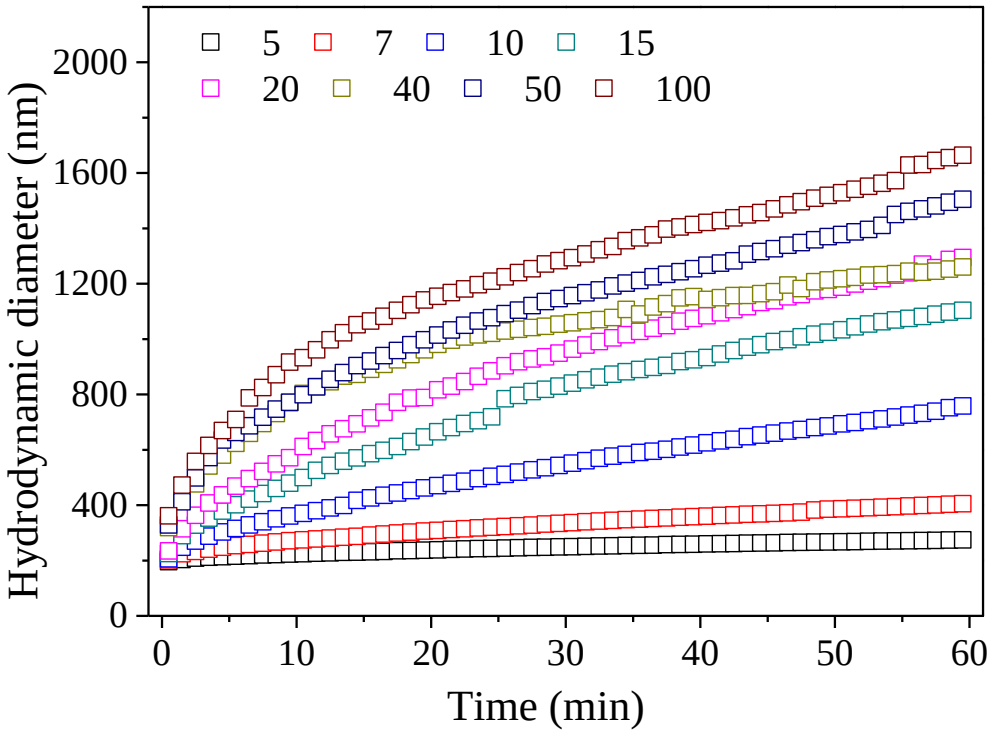

Figure S29. Time-evolution hydrodynamic diameters of colloidal minerals in KH_2PO_4 solutions. The electrolyte concentrations (mmol/L) are indicated in the legend.

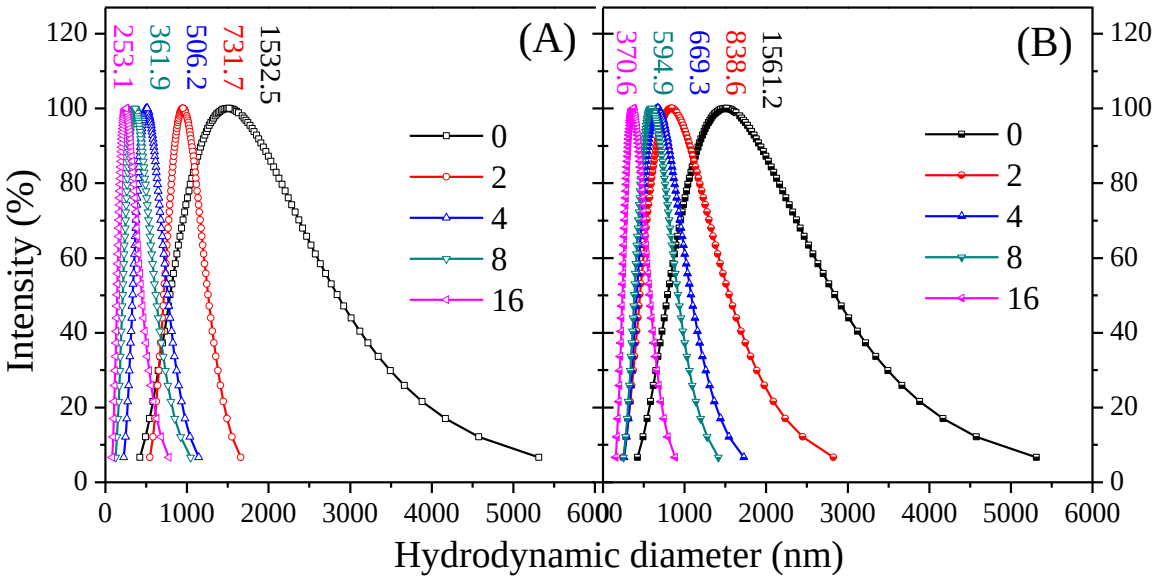

Figure S30. Effect of dilution ratios on the hydrodynamic diameters of colloidal minerals in (A) 80 mmol/L KOH solutions (pH = 12.7); (B) 70mmol/L KNO_3 solutions (pH = 8). The dilution ratios are 2, 4, 8 and 16 as indicated in the legends. The data at the top of the curves are hydrodynamic diameters of aggregates after dilutions.